Supporting Information

Boosting the Photocatalytic Performance of $BiVO_4$ via Plasmonic AgCu Alloy Engineering

Mingze Xu,[*a] Chang Su,[a] Hongyuan Xie,[a] Tingsong Zhang,[a] Yongze Gao[b] and Wenzhe Si[*b]

a. Nanophotonics and Biophotonics Key Laboratory of Jilin Province, Changchun University of Science and Technology, Changchun, 130022, China
b. Key Laboratory of Groundwater Resources and Environment (Jilin University), Ministry of Education, College of New Energy and Environment, Jilin University, Changchun 130021, China.

EXPERIMENT

Synthesis of catalyst

The schematic diagram illustrating the preparation process of AgCu-$BiVO_4$ material is provided in Fig. S1. Silver nitrate ($AgNO_3$, analytical grade, Beijing Dingguo Changsheng Biotechnology Co., Ltd.) and copper(II) acetate ($Cu(CH_3COO)_2$, analytical grade, Tianjin Fangchen Fangzheng Chemical Reagent Factory) were mixed in a molar ratio of Ag:Cu = 1:2 (excessive copper), corresponding to an excess of Cu. This mixture was then combined with bismuth vanadate ($BiVO_4$, 99%, Guangdong Qianjin Chemical Reagent Co., Ltd.) at a molar ratio of metal precursors to $BiVO_4$ of 1:6, and dispersed in ethylene glycol (98%, Macklin). Polyvinylpyrrolidone K30 (PVP, GR grade, Sinopharm Chemical Reagent Co., Ltd.) was added as a dispersant at a mass ratio of 2:1 relative to the total metal precursor salts. The resulting suspension was heated under continuous stirring for 30 to 90 min. After the reaction, the product was collected by centrifugation, washed three times with a 1:1 (v/v) mixture of ethanol and deionized water, and dried in a vacuum oven at 80 °C for 14 h. The dried powder

was subsequently ground to obtain the AgCu nanoparticle-decorated $BiVO_4$ (AgCu-$BiVO_4$). nanocomposite.

The Ag-$BiVO_4$ nanocomposite, serving as a reference for AgCu-$BiVO_4$, was prepared under exactly the same synthetic conditions. The sole variable was the precursor composition: only the Ag precursor was introduced, with no addition of a Cu precursor.

Catalysts characterization

The phase structure of all samples was analyzed by X-ray diffraction (XRD, Rigaku D/MAX 2550 v/PC, Japan Cu-Kα radiation, λ = 0.15418 nm) patterns. The morphology of the samples were observed by Transmission electron microscope (TEM, JEM-2100, Japan). X-ray photoelectron spectroscopy (XPS) of all samples were obtained on an X-ray photoelectron spectrometer (ESCALAB 250XI). The ultraviolet-visible (UV–vis) diffuse reflectance spectrums were achieved on a UV–vis spectrophotometer (Agilent Technologies). Photoluminescence (PL) was measured on the RF-5301PC (Shimadzu, Japan). The carrier lifetimes of $BiVO_4$ and AgCu-$BiVO_4$ were investigated using an ultrafast fluorescence lifetime spectrometer (FLS980).

Photoelectrochemical measurements

Electrochemical measurements were carried out in a 0.1 M Na_2SO_4 aqueous electrolyte using a Cortest CS350 electrochemical workstation (Cortest Instruments, China). A standard three-electrode configuration was employed, consisting of the prepared sample as the working electrode, a platinum wire as the counter electrode, and an Ag/AgCl (saturated KCl) reference electrode. A 300 W xenon arc lamp served as the light source for photoelectrochemical tests. The working electrode was fabricated by depositing the photocatalyst onto a 1 cm × 1 cm indium tin oxide (ITO)-coated glass substrate. In a typical procedure, 40 mg of the as-synthesized sample was dispersed in 2 mL of ethanol, followed by the addition of 10 μL of Nafion solution (5 wt%). The resulting suspension was ultrasonicated for 30 min to ensure homogeneity. Subsequently, 20 μL of the ink was drop-cast onto the ITO surface and spin-coated in

two steps: first at 1000 rpm for 15 s, then at 2000 rpm for another 15 s. This deposition process was repeated three times to achieve uniform catalyst loading. The coated electrode was then dried in ambient air for 24 h prior to testing. Transient photocurrent responses were recorded under chopped illumination, and linear sweep voltammetry (LSV) measurements were performed in the potential window of −0.8 to −2.0 V versus Ag/AgCl at a scan rate of 10 mV s^{-1}.

Photocatalytic activity

The photocatalytic activity of AgCu-$BiVO_4$ was evaluated by monitoring the degradation of Rhodamine 6G (Rh6G) under simulated solar irradiation. Specifically, the as-prepared AgCu-$BiVO_4$ photocatalyst was dispersed in 100 mL of an aqueous Rh6G solution (5 mg L^{-1}). Prior to illumination, the suspension was stirred in the dark for 30 min to establish adsorption–desorption equilibrium. Photocatalytic degradation was then initiated using a 300 W xenon arc lamp positioned 0.5 m above the reaction vessel, equipped with a UV cutoff filter ($\lambda \geq 420$ nm) to eliminate ultraviolet light. To exclude thermal effects, the reaction temperature was maintained at 25 °C throughout the experiment using a thermostatic water circulator. Aliquots (ca. 3 mL) were collected at 10-min intervals, immediately centrifuged to remove photocatalyst particles, and analyzed via UV–Vis spectrophotometry. The absorbance of the supernatant at the characteristic wavelength of Rh6G ($\lambda_{max} \approx 526$ nm) was recorded. A calibration curve based on the Beer–Lambert law confirmed a linear relationship between Rh6G concentration and absorbance under the experimental conditions; thus, the temporal evolution of absorbance was used to quantify the degradation efficiency.

DFT calculations

Based on the experimental characterization of the photocatalytically optimal AgCu-$BiVO_4$ composite, the initial computational model was constructed as follows: monoclinic $BiVO_4$ was modeled with a supercell exposing the (−1 3 0) facet as the dominant surface, consistent with high-resolution TEM observations; the AgCu alloy was modeled in an Ag-type face-centered cubic (fcc) lattice with an atomic Ag:Cu ratio

of 3:1 and preferentially terminated by the (111) facet to reflect its experimentally observed morphology and composition. Theoretical calculations were carried out based on periodic DFT using the Vienna ab initio simulation package (VASP 6.3.2). To describe electron-ion interactions, scalar relativistic effect projector-augmented waves (PAW) methods were used in conjunction with generalized gradient approximation (GGA) and Perdew-Burke-Ernzerhof (PBE) functionals to handle electron exchange and related energy. For the planewave basis set, a kinetic energy cutoff of 400 eV was employed. The convergence threshold of 1×10^{-5} eV was set for the electronic energy and ionic relaxation proceeded until the atomic force was less than 0.05 $eV \cdot Å^{-1}$. Grimme's approach (DFT + D3) was incorporated to mimic the van der Waals interactions and dispersion-energy corrections. Meanwhile, dipole corrections along the surface normal direction were included by setting IDIPOL = 3. The Monkhorst–Pack grid was used to sample the first Brillouin zone. The $2 \times 2 \times 1$ k-point mesh was adopted for electronic structures analysis and geometric optimization. Hubbard U was used to modify the strong on-site Coulombic interaction between d orbitals of the transition elements, as well as that between the p orbitals of Bi, where the Ueff (U-J) of V, Cu, Ag and Bi were 5.0 eV, 4.0 eV, 3.5 eV and 3.0 eV, respectively.

Table S1 Rate constants (k) for RhB degradation by different catalysts

	k1 (10^{-2} min^{-1})	k2 (10^{-2} min^{-1})	k_{avg} (10^{-2} min^{-1})
$BiVO_4$	-	-	0.39
Ag-$BiVO_4$	-	-	0.45
Ag_7Cu_1-$BiVO_4$	0.90	1.63	1.26
Ag_3Cu_1-$BiVO_4$	1.36	3.98	2.67
Ag_1Cu_1-$BiVO_4$	1.02	1.90	1.40

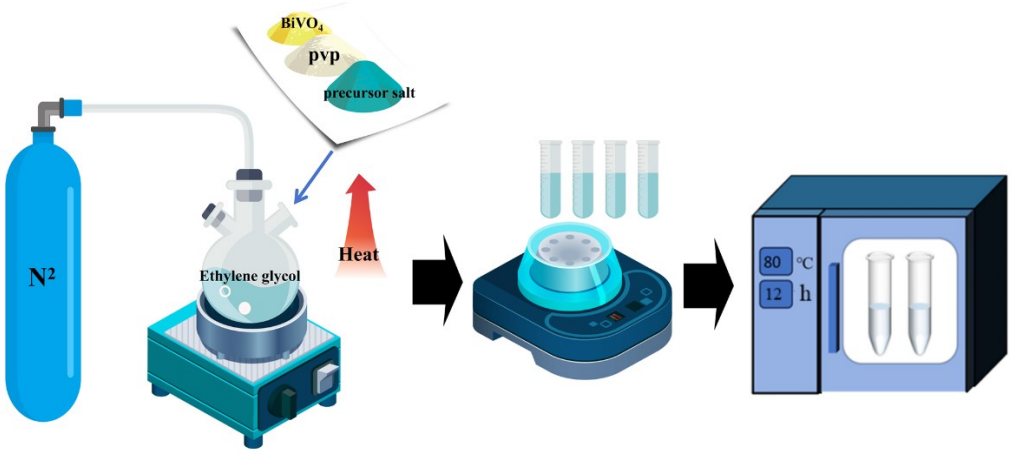

Fig. S1. Schematic diagram of preparation process for AgCu-$BiVO_4$

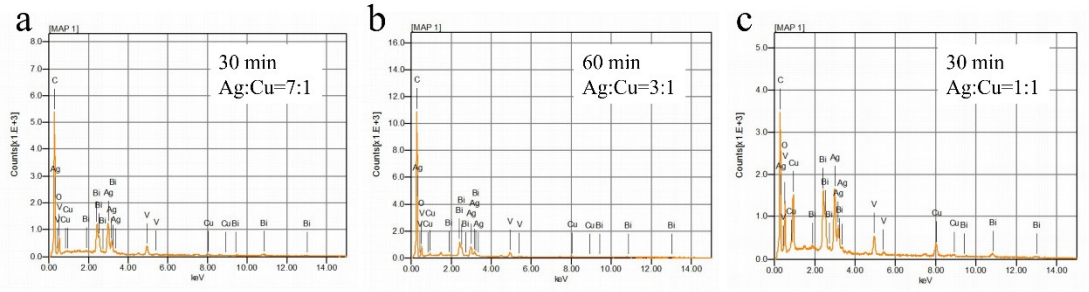

Fig. S2. EDS diagrams of AgCu-$BiVO_4$ samples prepared by different times

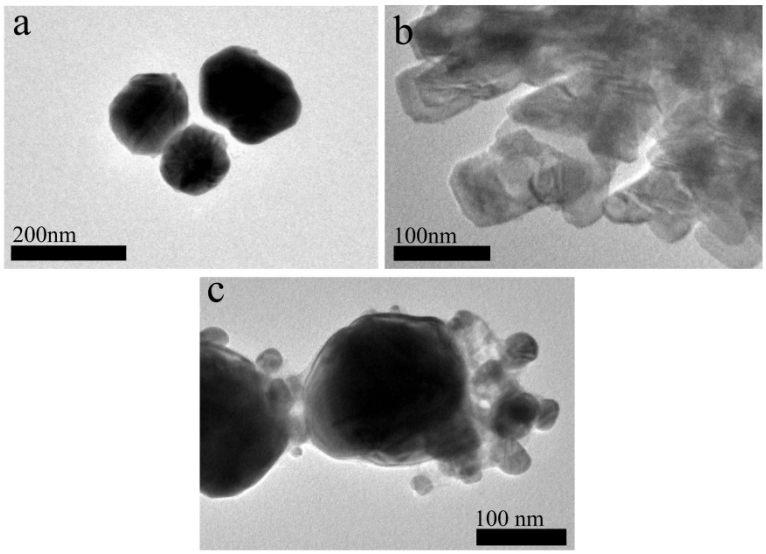

Fig. S3. TEM images of AgCu nanoparticles (a), $BiVO_4$ (b) and Ag-$BiVO_4$ (c)

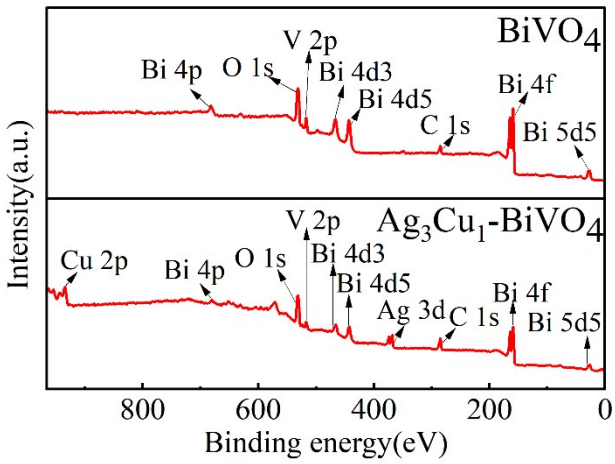

Fig. S4. Full XPS spectrum of $BiVO_4$ and Ag_3Cu_1-$BiVO_4$

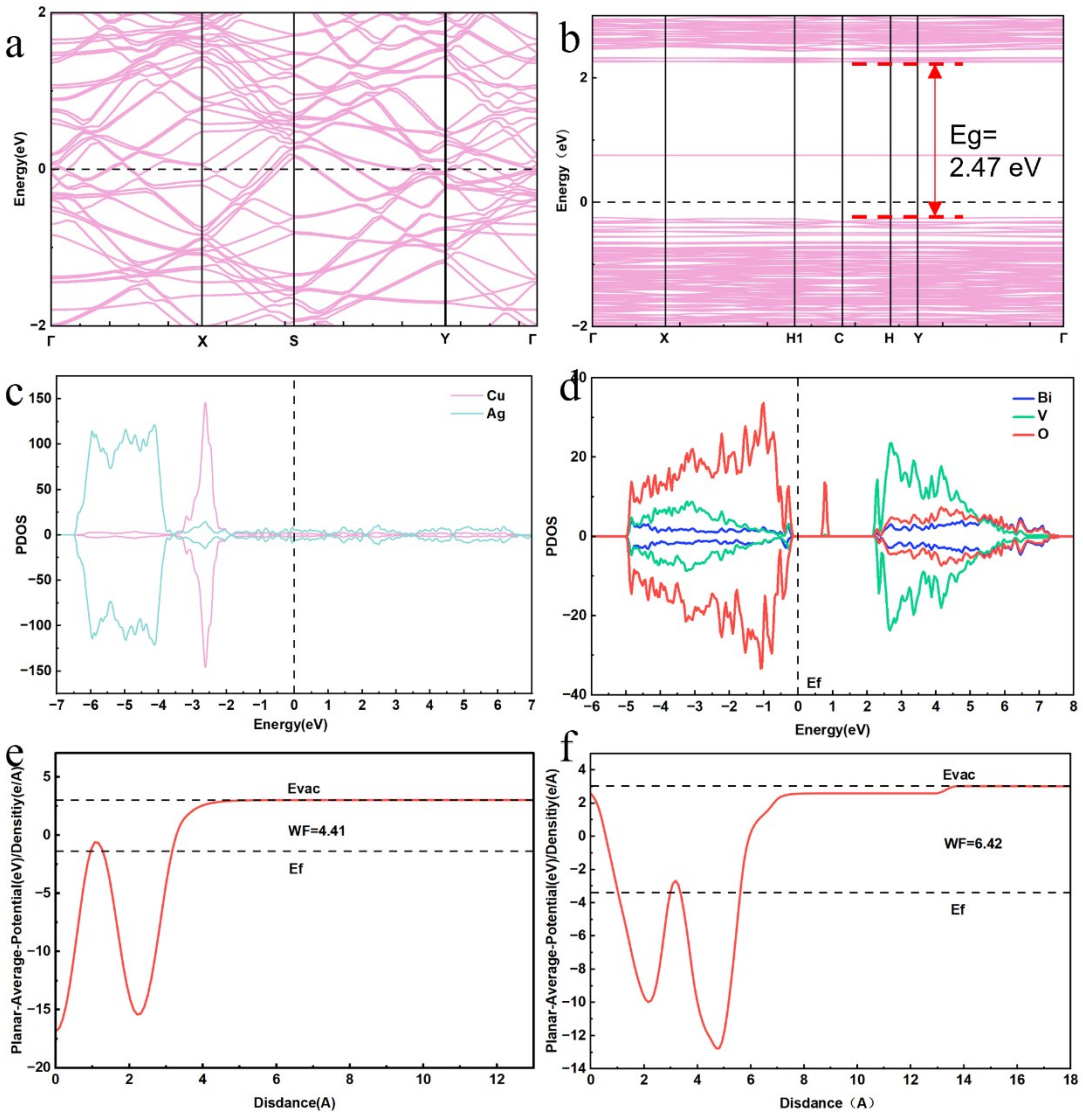

Fig. S5. (a, b) Band structures, (c, d) density of states, and (e, f) electrostatic potential profiles of (a, c, e) AgCu alloy and (b, d, f) $BiVO_4$, calculated by density functional theory.

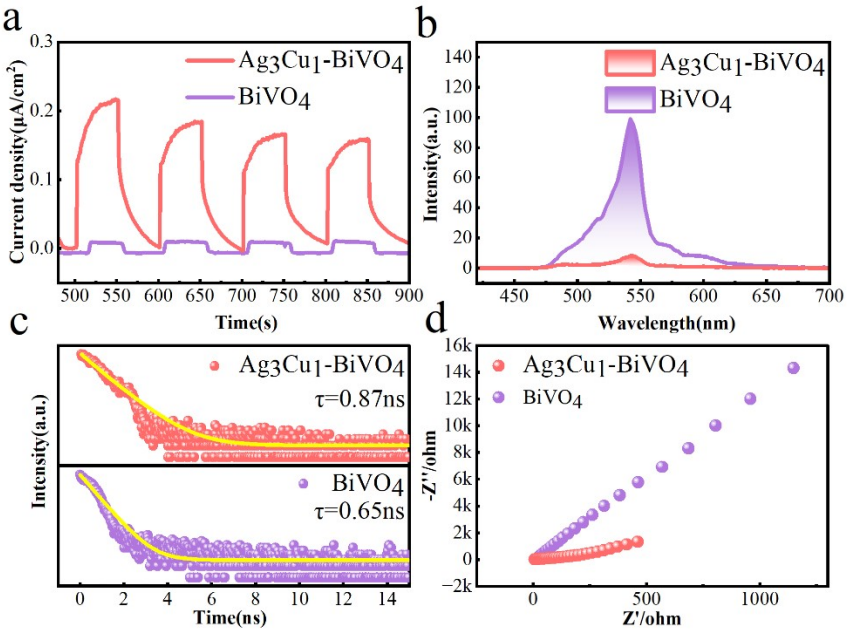

Fig. S6. Photocurrent response (a), photoluminescence spectra (b), fitted time-resolved fluorescence decay profiles (c), and electrochemical impedance spectroscopy (EIS) Nyquist plots (d) of $BiVO_4$ and Ag_3Cu_1-$BiVO_4$.